

# Mutually exciting point process graphs for modelling dynamic networks

Francesco Sanna Passino and Nicholas A. Heard

Department of Mathematics, Imperial College London  
180 Queen's Gate, SW7 2AZ, London

## Abstract

A new class of models for dynamic networks is proposed, called mutually exciting point process graphs (MEG), motivated by a practical application in computer network security. MEG is a scalable network-wide statistical model for point processes with dyadic marks, which can be used for anomaly detection when assessing the significance of previously unobserved connections. The model combines mutually exciting point processes to estimate dependencies between events and latent space models to infer relationships between the nodes. The intensity functions for each network edge are parameterised exclusively by node-specific parameters, which allows information to be shared across the network. Fast inferential procedures using modern gradient ascent algorithms are exploited. The model is tested on simulated graphs and real world computer network datasets, demonstrating excellent performance.

**Keywords** — dynamic network, Hawkes process, self-exciting process, statistical cyber-security.

## 1 Introduction

Dynamic networks are encountered in many domains, for example representing interactions in social networks, messaging applications, or computer networks. Event data from dynamic networks are observed as triplets  $(t_1, x_1, y_1), \dots, (t_m, x_m, y_m)$ , where  $0 \leq t_1 \leq t_2 \leq \dots$  are event times and the dyadic marks  $(x_k, y_k)$  denote the source and destination nodes, each belonging to a set of nodes  $V = \{1, \dots, n\}$  of size  $n$ . The sequence of graph edges  $(x_1, y_1), \dots, (x_m, y_m)$  induces a directed *network adjacency matrix*  $\mathbf{A} = \{A_{ij}\} \in \{0, 1\}^{n \times n}$  where  $A_{ij} = 1$  if node  $i$  connected to node  $j$  at least once during the entire observation period, and  $A_{ij} = 0$  otherwise.

This article presents a new model for the arrival of connection events between nodes in a network, motivated by applications in computer network security. Modelling arrival times in computer networks is complicated by several factors: events tend to appear in bursts, they might be recorded multiple times, and exhibit polling at regular intervals (Heard et al., 2014). Furthermore, in computer network security, it is particularly important to assess the significance of observing *new links*, corresponding to connections on previously unobserved edges (Metelli and Heard, 2019). New links might be indicative of lateral movement, which is a common behaviour of network attackers (Neil et al., 2013). The proposed *mutually exciting graphs* (MEG) framework for modelling point processes on networks simultaneously addresses two fundamental tasks in network security: monitoring the normality of observed connectivity traffic, and anomaly detection for unusual new connections. Despite the focus of this article on applications

to computer network security, the proposed methodology is general and can be applied to *any* dynamic network expressed as a point process with dyadic marks.

The MEG model builds upon mutually exciting point processes and latent space models. Mutually exciting point processes have been already successfully used for a variety of different applications: modelling of earthquakes (Ogata, 1988), financial markets (Bowsher, 2007), criminal activities (Mohler et al., 2011; Stomakhin et al., 2011), and popularity of tweets (Zhao et al., 2015; Chen and Tan, 2018). Let  $t_1, t_2, \dots, t_m$  denote an increasing sequence of observed event times, and  $N(t) = \sum_{k=1}^m \mathbb{1}_{[0,t]}(t_k)$  the corresponding counting process, representing the number of events observed up to time  $t$ . The conditional intensity  $\lambda(t)$  is assumed to depend on the last  $r$  observed arrival times:

$$\lambda(t) = \lambda + \sum_{k>N(t)-r}^{N(t)} \omega(t - t_k), \quad (1.1)$$

where  $\lambda \in \mathbb{R}_+$  is a baseline intensity level and  $\omega(\cdot)$  is a non-increasing and non-negative excitation function. For simplicity,  $\omega(\cdot)$  is usually chosen to be a scaled exponential function:  $\omega(t) = \beta \exp\{-(\beta + \theta)t\}$ , where  $\beta \geq 0$  and  $\theta > 0$ . Alternative choices of  $\omega(\cdot)$  are nonparametric step functions (Price-Williams and Heard, 2020), or the power-law  $\omega(t) = \theta(t + \gamma)^{-1-\delta}$ , where  $\theta \geq 0$ ,  $\beta, \delta > 0$  and  $\theta < \delta\beta^\delta$  (Ozaki, 1979). In the literature, two extreme cases for the intensity in (1.1) are usually considered:  $r = 1$ , corresponding to a first order Markov-like structure, and  $r = \infty$ , called a Hawkes process (Hawkes, 1971). If  $r = 0$ , the model reduces to a Poisson process. Price-Williams and Heard (2020) showed that self-exciting point processes appear to be suitable for modelling arrival times on *individual* network edges in a cyber-security application. In this article, an extension of this approach is proposed, aimed at modelling network data, and, more generally, point processes with dyadic marks.

In large graphs, simultaneously modelling all the edge processes using individual intensities of the form (1.1) is computationally challenging, and ignores possible correlations between different edges and nodes. Inference would require estimating  $\mathcal{O}(n^2)$  parameters, or  $\mathcal{O}\{\text{nnz}(\mathbf{A})\}$  parameters if the graph is sparse, which is not feasible in most real-world applications. Furthermore, this approach would not parameterise *new edges* appearing after the model training period. Hence, traditional statistical models for networks, for example the *latent space models* (Hoff et al., 2002), aim to reduce the representation of the network to  $\mathcal{O}(n)$  parameters. Inspired by the literature on latent space models, here a dynamic graph is modelled through the edge-specific point processes with intensity functions parametrised by node-specific latent features. In standard latent space network models, the probability of a link between two nodes is expressed as a function of node-specific latent vectors  $\mathbf{a}_i, \mathbf{b}_j \in \mathbb{R}^d$ , such that  $\mathbb{P}(A_{ij} = 1) = f(\mathbf{a}_i, \mathbf{b}_j)$ , for some kernel function  $f$ . Similarly, here it is assumed that the arrival times on each observed network edge can be modelled using a mutually exciting point process depending on node-specific characteristics.

The related literature on mutually exciting point processes is vast, although mostly focusing on univariate and multivariate point processes; limited attention is devoted to using such processes for modelling large dynamic graphs. Hawkes processes are traditionally used to estimate causal interactions within multivariate processes (Linderman and Adams, 2014), because of their appealing theoretical properties in terms of Granger causality and directed information (Etesami et al., 2016; Eichler et al., 2017). The approach proposed in this paper is related to Perry and Wolfe (2013), who consider directed interaction within dynamic networks as a multivariate point process using a Cox multiplicative intensity model, with covariates depending on the history of the process. The methodology proposed in this work uses mutually exciting processes parametrised by node-specific features. Hawkes processes have also been used in Fox et al. (2016) to analyse e-mail networks, primarily focusing on point processes on each node.

Furthermore, dynamic models for network snapshots observed at *discrete* points in time have also been proposed in the literature. In particular, the methodology proposed in this work could be related to

*dynamic latent space models*, which are based on latent feature representations of each node, evolving according to a temporal dynamics. Examples are [Sarkar and Moore \(2006\)](#); [Krivitsky and Handcock \(2014\)](#); [Sewell and Chen \(2015\)](#); [Durante and Dunson \(2016\)](#). The MEG model proposed in this article extends the latent feature framework to a continuous time setting, using node-specific latent vectors to parametrise point processes on each edge.

The remainder of this article is structured as follows: Section 2 introduces the MEG model and related inferential procedures. Section 3 discusses simulation from the model and the calculation of  $p$ -values for each observed network event. Results on simulated and real-world computer networks are discussed in Section 4.

## 2 Mutually exciting point process graphs

The main contribution proposed in this article is a *mutually exciting graph model* (MEG) for dynamic network point processes, defined by an  $n \times n$  time-varying matrix of non-negative functions  $\lambda(t) = \{\lambda_{ij}(t)\}$ . Each entry  $\lambda_{ij}(t)$  represents the intensity of the counting process  $N_{ij}(t) = \sum_{k=1}^m \mathbb{1}_{[0,t] \times \{i\} \times \{j\}}(t_k, x_k, y_k)$  of events occurring on the graph edge  $(i, j)$ . For generality, it is assumed that for each edge  $(i, j)$  there exists a changepoint  $\tau_{ij} \geq 0$  after which the edge becomes observable. In the simplest case,  $\tau_{ij} = 0 \forall i, j$ .

To parameterise  $\lambda(t)$ , each entry is represented as an additive model with three non-negative components. The first, denoted  $\alpha_i(t)$ , characterises the process of arrival times involving  $i$  as source node; the second,  $\beta_j(t)$ , corresponds to arrivals for which  $j$  is the destination node; the third,  $\gamma_{ij}(t)$ , is an interaction term which will also be parameterised by node-specific parameters, giving:

$$\lambda_{ij}(t) = \alpha_i(t) + \beta_j(t) + \gamma_{ij}(t), \quad t \geq \tau_{ij}. \quad (2.1)$$

Note that the intensity function (2.1) resembles the link function used in *additive and multiplicative effect network* (AMEN) models for network adjacency matrices, proposed in [Hoff \(2018\)](#).

Define the source and destination counting processes as  $N_i(t) = \sum_{k=1}^m \mathbb{1}_{[0,t] \times \{i\}}(t_k, x_k)$  and  $N'_j(t) = \sum_{k=1}^m \mathbb{1}_{[0,t] \times \{j\}}(t_k, y_k)$ . Furthermore, let  $\ell_{i1}, \ell_{i2}, \dots$  denote the indices  $\{k : x_k = i\}$  of the arrival times such that  $i$  appears as source node, and  $\ell'_{j1}, \ell'_{j2}, \dots$  denote the event indices  $\{k : y_k = j\}$  for which  $j$  is the destination node. To allow self excitation of both source and destination nodes, the latent functions  $\alpha_i(t)$  and  $\beta_j(t)$  are assigned a similar form to the conditional intensity (1.1):

$$\alpha_i(t) = \alpha_i + \sum_{k > N_i(t) - r}^{N_i(t)} \omega_i(t - t_{\ell_{ik}}), \quad \beta_j(t) = \beta_j + \sum_{k > N'_j(t) - r}^{N'_j(t)} \omega'_j(t - t_{\ell'_{jk}}), \quad (2.2)$$

where  $\alpha = (\alpha_1, \dots, \alpha_n), \beta = (\beta_1, \dots, \beta_n) \in \mathbb{R}_+^n$  are node-specific baseline intensity levels, and  $\omega_i, \omega'_i$  are node-specific, non-increasing excitation functions from  $\mathbb{R}_+$  to  $\mathbb{R}_+$ . For simplicity, the excitation functions assume the following scaled exponential form, for non-negative parameters  $\mu_i, \mu'_i, \phi_i, \phi'_i \in \mathbb{R}_+^n$ :

$$\omega_i(t) = \mu_i \exp\{-(\mu_i + \phi_i)t\}, \quad \omega'_i(t) = \mu'_i \exp\{-(\mu'_i + \phi'_i)t\}. \quad (2.3)$$

Similarly, let  $\ell_{ij1}, \ell_{ij2}, \dots$  be the indices  $\{k : x_k = i, y_k = j\}$  of the events observed on the edge  $(i, j)$ . The interaction term  $\gamma_{ij}(t)$  in (2.1) assumes a similar form to (2.2), but with a background rate obtained as the inner product between two node-specific  $d > 0$ -dimensional baseline parameter vectors  $\gamma_i, \gamma'_j \in \mathbb{R}_+^d$ :

$$\gamma_{ij}(t) = \gamma_i \cdot \gamma'_j + \sum_{k > N_{ij}(t) - r}^{N_{ij}(t)} \omega_{ij}(t - t_{\ell_{ijk}}), \quad (2.4)$$

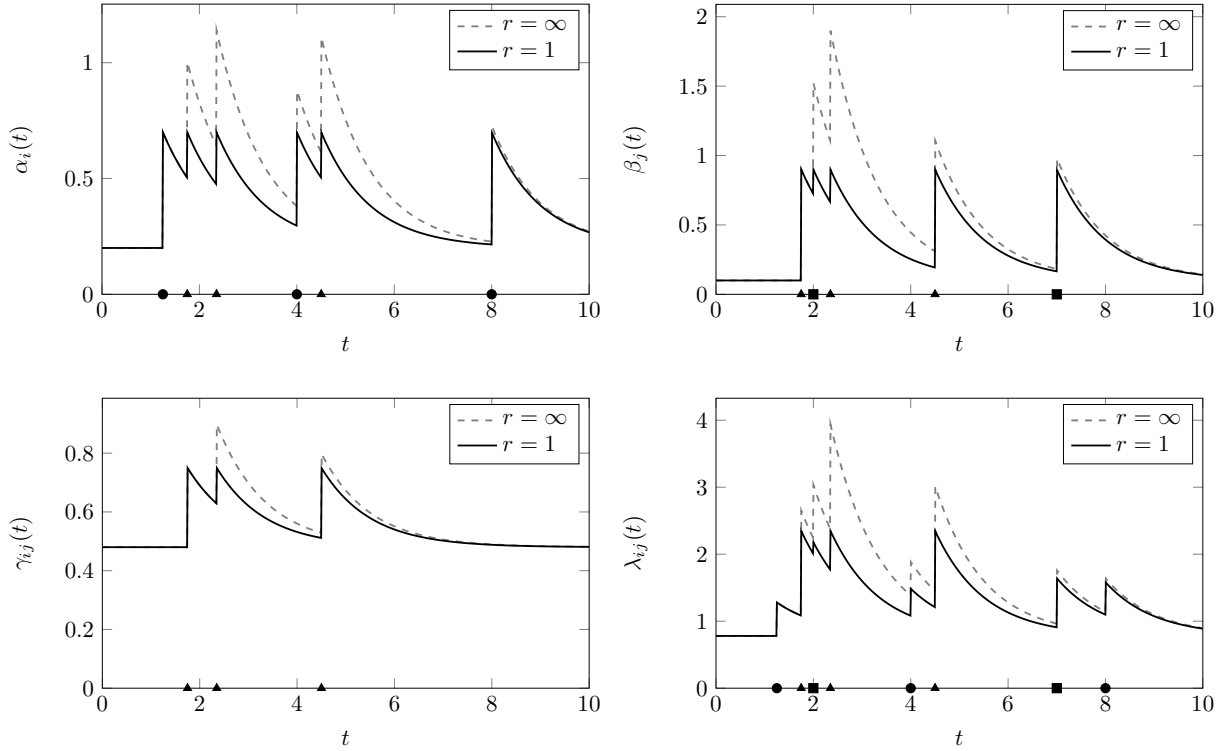


**Figure 1:** Cartoon of a 1-dimensional MEG model (2.1)–(2.5). Events with source node  $i$  and destination node  $j$  are denoted by triangles; other events with source node  $i$  are denoted with circles, and other events with destination node  $j$  are denoted by squares.

The inner product baseline is inspired by random dot product graph models (see, for example, [Athreya et al., 2018](#)) for link probabilities. The excitation function  $\omega_{ij}(t)$  is also expressed as a sum of scaled exponential functions, parameterised by four node-specific, non-negative latent  $d$ -vectors  $\nu, \nu', \theta_i, \theta'_j \in \mathbb{R}_+^d$ :

$$\omega_{ij}(t) = \sum_{\ell=1}^d \nu_{i\ell} \nu'_{j\ell} \exp\{-(\theta_{i\ell} + \nu_{i\ell})(\theta'_{j\ell} + \nu'_{j\ell})t\}. \quad (2.5)$$

A cartoon example of the intensity  $\lambda_{ij}(t)$  for the  $d = 1$  dimensional MEG model with scaled exponential functions is given in Figure 1, with  $\alpha_i = 0.2$ ,  $\mu_i = 0.5$ ,  $\phi_i = 0.5$ ,  $\beta_j = 0.1$ ,  $\mu'_j = 0.8$ ,  $\phi'_j = 0.2$ ,  $\gamma_i = 0.8$ ,  $\nu_i = 0.9$ ,  $\theta_i = 1.1$ ,  $\gamma'_j = 0.6$ ,  $\nu'_j = 0.3$ ,  $\theta'_j = 0.2$ .

As remarked in Section 1, alternative decay functions are possible, like nonparametric excitation functions ([Price-Williams and Heard, 2020](#)) or power-laws ([Ozaki, 1979](#)). In addition to the self-exciting component, non-stationary background rates are also considered in the literature, often with a seasonal component ([Fox et al., 2016](#); [Price-Williams and Heard, 2020](#)). In cyber-security applications, including seasonal components when modelling arrival times was demonstrated to have limited effect on the predictive performance of the model ([Price-Williams and Heard, 2020](#)); therefore, the background rate here is assumed to be constant.

A key feature of the model is the representation of the intensity (2.1) with only node-specific parameters  $\Psi = (\alpha, \mu, \phi, \beta, \mu', \phi', \gamma, \nu, \theta, \gamma', \nu', \theta')$ . This construction allows estimation of intensities even for unobserved edges. Therefore, in practical applications, when a new link is observed, it is possible to

immediately provide an estimate of the intensity of the process on that edge. This is a substantial difference with respect to models based on edge-specific parameters for the edge intensities. Such models do not perform well for scoring new links, since the score for a new observation could only be based on a prior guess of the intensity, whereas MEG “borrows strength” from events observed on similar nodes and edges in the graph, providing an informed estimate of the intensity function on the newly observed edge.

For a sequence of observed events  $\mathcal{H}_T = \{(x_1, y_1, t_1), \dots, (x_m, y_m, t_m)\}$ , with event times in  $[0, T]$ , the log-likelihood (Daley and Vere-Jones, 2002) of a generic MEG model is:

$$\log L(\mathcal{H}_T | \Psi) = \sum_{i=1}^n \sum_{j=1}^n \left\{ \sum_{k=1}^{n_{ij}} \log \lambda_{ij}(t_{\ell_{ijk}}) - \int_{\tau_{ij}}^T \lambda_{ij}(t) dt \right\}. \quad (2.6)$$

where  $n_{ij}$  is the number of events observed on edge  $(i, j)$ . Explicit forms of the likelihood function (2.6) for the scaled exponential excitation function model, with  $d = 1$  and  $r = 1$  or  $r = \infty$ , are discussed in Appendix A.1.

For  $r = \infty$ , the main computational burden associated with the calculation of the likelihood (2.6) is the double summation over each  $(i, j)$  pair of the sum of intensities  $\lambda_{ij}(t_{\ell_{ijk}})$  for the events  $t_{\ell_{ijk}}$ , and the summations required in (2.2) and (2.4) to evaluate that intensity for each event. Appendix A.1 discusses a recursive form of the likelihood (2.6) for the MEG model with  $r = \infty$ , which can be evaluated in linear time on each active edge, significantly reducing the computational effort.

## 2.1 Inference via gradient ascent methods

Inference in Hawkes processes is usually carried out using maximum likelihood estimation, and for MEG models maximum likelihood estimation via gradient ascent can be deployed, since it is not possible to optimise (2.6) analytically. If the start times  $\tau_{ij}$  in (2.6) are unknown, the maximum likelihood estimates are simply  $\hat{\tau}_{ij} = t_{\ell_{ij1}}$  if at least one event is observed on the edge, and  $\hat{\tau}_{ij} = \infty$  otherwise (see Appendix A.1). For maximising (2.6) with respect to the remaining parameters  $\Psi$ , the adaptive moment estimation method (Adam, Kingma and Ba, 2015) is used with a minor adaptation of optimising the logarithm of each parameter since are all constrained to be positive. The resulting optimisation procedure is detailed in Algorithm 1. Alternative gradient ascent techniques for optimisation are surveyed in Ruder (2016). The gradient of the likelihood (2.6) with respect to  $\Psi$  is explicitly derived in Appendix A.2 for  $d = 1$  and  $r = \infty$ .

## 2.2 Extension to undirected and bipartite graphs

The proposed modelling framework has been presented for directed graphs, but could be easily extended to undirected and bipartite networks. For undirected graphs  $\mathbf{A} = \mathbf{A}^\top$ , hence there is no distinction between source and destination nodes. Therefore,  $\beta_j(t)$  in (2.1) could be simply be replaced by  $\alpha_j(t)$ , and  $\gamma_{ij}(t)$  modified as follows:

$$\gamma_{ij}(t) = \gamma_i \cdot \gamma_j + \sum_{k > N_{ij}(t) - r}^{N_{ij}(t)} \sum_{\ell=1}^d \nu_{i\ell} \nu_{j\ell} \exp\{-(\theta_{i\ell} + \nu_{i\ell})(\theta_{j\ell} + \nu_{j\ell})t\}.$$

Furthermore, bipartite graphs can be considered as special cases of directed graphs, where the node set  $V = V_1 \cup V_2$  is divided into two sets  $V_1$  and  $V_2$  of cardinality  $n_1$  and  $n_2$ , such that  $V_1 \cap V_2 = \emptyset$ , and all the edges are of the form  $(i, j)$  with  $i \in V_1$  and  $j \in V_2$ . Therefore, (2.1) and the corresponding equations of the intensity functions still hold, assuming that  $i \in V_1$  and  $j \in V_2$ .

---

**Algorithm 1:** *Adam* gradient ascent algorithm for optimisation of the likelihood (2.6).

---

**Input:** stepsize  $\eta \in \mathbb{R}_+$ , decay rates  $\rho_1, \rho_2 \in (0, 1)$ , smoothing term  $\varepsilon \in \mathbb{R}_+$ , initial values  $\Psi_0$ .

**Output:** model parameters  $\Psi$ .

- 1 Initialise the moment vectors  $\mathbf{m}$  and  $\mathbf{v}$ , and the number of iterations  $k$ :  $\mathbf{m}_0 \leftarrow \mathbf{0}, \mathbf{v}_0 \leftarrow \mathbf{0}, k \leftarrow 0$ ,
  - 2 **repeat**
  - 3      $k \leftarrow k + 1$ ,
  - 4      $\mathbf{g}_k \leftarrow \frac{\partial}{\partial \Psi} \log L(\mathcal{H}_T | \Psi) \Big|_{\Psi = \Psi_{k-1}}$ ,
  - 5      $\mathbf{m}_k \leftarrow \rho_1 \mathbf{m}_{k-1} + (1 - \rho_1)(\mathbf{g}_k \odot \Psi_{k-1})$ , where  $\odot$  is the Hadamard product,
  - 6      $\mathbf{v}_k \leftarrow \rho_2 \mathbf{v}_{k-1} + (1 - \rho_2)[(\mathbf{g}_k \odot \Psi_{k-1}) \odot (\mathbf{g}_k \odot \Psi_{k-1})]$ ,
  - 7      $\Psi_k \leftarrow \Psi_{k-1} \odot \exp \left\{ \eta \mathbf{m}_k / (1 - \rho_1^k) \oslash \left( \sqrt{\mathbf{v}_k / (1 - \rho_2^k)} + \varepsilon \right) \right\}$ , where  $\oslash$  is the Hadamard division, and the exponential and square root are applied element-wise,
  - 8 **until** convergence in  $\log L(\mathcal{H}_T | \Psi)$ ;
- 

### 3 Simulation and assessment of the goodness-of-fit

In order to validate the inferential procedure, it is necessary to simulate data from the MEG model (2.1), which can be interpreted as an extended multivariate Hawkes process where some of the parameters are shared across the individual processes. Therefore, simulation of MEG models is possible under the framework described in Ogata (1981), and follows the standard technique of simulating self-exciting processes via *thinning*. The procedure is described in Algorithm 2.

---

**Algorithm 2:** Simulation of a MEG in  $[0, T]$ .

---

- 1 set  $t^* = 0$ ,
  - 2 **repeat**
  - 3     set  $\lambda^* = \sum_{i=1}^n \sum_{j=1}^n \lambda_{ij}(t_+^*)$ , where  $t_+^*$  denotes the limit from the right,
  - 4     generate the inter-arrival time  $q = -\log(u)/\lambda^*$ , where  $u$  is a draw from Uniform $[0, 1]$ ,
  - 5     obtain the candidate arrival time  $t^* \leftarrow t^* + q$ ,
  - 6     assign the arrival time  $t^*$  to the edge  $(i, j)$  with probability  $\lambda_{ij}(t_-^*)/\lambda^*$ , and do not assign to any edge with probability  $1 - \sum_{i=1}^n \sum_{j=1}^n \lambda_{ij}(t_-^*)/\lambda^*$ , where  $t_-^*$  denotes the limit from the left.
  - 7 **until**  $t^* > T$ ;
- 

Furthermore, it is possible to assess the performance of the inferential procedure by evaluating the goodness-of-fit from out-of-sample events. If the model parameters are estimated only from the event times obtained in  $[0, T^*]$ , with  $T^* < T$ , using Algorithm 1, the goodness-of-fit can then be evaluated from the event times in  $(T^*, T]$ . Goodness-of-fit measures can be calculated from functions of the compensator function for the model. Given the conditional intensity  $\lambda_{ij}(t)$ , the compensator  $\Lambda_{ij}(t)$  is:

$$\Lambda_{ij}(t) = \int_{\tau_{ij}}^t \lambda_{ij}(s) ds.$$

Examples of compensator functions for some MEG models, for  $t = T$ , can be found in Appendix A.1. Given arrival times  $t_1, \dots, t_{n_{ij}}$  on the edge  $(i, j)$ , under the null hypothesis of correct specification of the conditional intensity  $\lambda_{ij}(t)$ , by time rescaling theorem (see, for example, Brown et al., 2002)



$\Lambda_{ij}(t_1), \dots, \Lambda_{ij}(t_{n_{ij}})$  are event times of a homogeneous Poisson process with unit rate. It follows that, for example, the upper tail  $p$ -values

$$p_k = \exp\{-\Lambda_{ij}(t_k) + \Lambda_{ij}(t_{k-1})\} = \exp\left\{-\int_{t_{k-1}}^{t_k} \lambda_{ij}(s) ds\right\} \quad (3.1)$$

follow a standard uniform distribution under the null hypothesis. Therefore, given the estimates of the conditional intensity functions obtained from the arrival times in  $[0, T^*]$ , approximately uniform  $p$ -values for the test event times in  $(T^*, T]$  should be observed if the model is specified and estimated correctly.

## 4 Applications and results

In this section, the MEG model is tested on simulated network data and on two real world computer network datasets: the Enron e-mail network, and a bipartite graph obtained from network flow data collected at Imperial College London. Across the experiments, the decay rates  $(\rho_1, \rho_2)$  in Algorithm 1 have been set to  $(0.9, 0.99)$ , and  $\varepsilon = 10^{-8}$ .

### 4.1 Simulated data

In order to evaluate Algorithm 1 and its performance at estimating MEG models, simulated network data are initially used. First, an adjacency matrix is simulated from an Erdős-Rényi graph with  $n = 10$  nodes, such that  $A_{ij} \sim \text{Bernoulli}(p)$ , with  $p = 1/4$ . For the edges such that  $A_{ij} = 1$ , then  $\tau_{ij} = 0$ , otherwise if  $A_{ij} = 0$ , then  $\tau_{ij} = \infty$ . Second,  $m = 5,000$  event times are generated from a MEG model with  $r = \infty$  using Algorithm 2, with parameters in  $\Psi$  sampled at random from uniform distributions, restricted to the following ranges:  $\alpha_i, \beta_j \in (10^{-5}, 10^{-4})$ ,  $\mu_i, \mu'_j, \phi_i, \phi'_j \in (10^{-5}, 10^{-3})$ ,  $\gamma_{il}, \gamma'_{j\ell} \in (10^{-5}, 10^{-1})$ ,  $\nu_{il}, \nu'_{j\ell}, \theta_{il}, \theta'_{j\ell} \in (10^{-2}, 10)$ . In the simulation, the expected number of events per active edge is  $mp/[n(n-1)] \approx 222$ . Algorithm 1 is used to estimate  $2n \times 6 = 120$  parameters, with learning rate  $\eta = 0.1$ , after a random initialisation from the same uniform distributions used in the data generating process. Using the estimated parameters, the  $p$ -values (3.1) are then calculated for all the simulated events. Finally, the Kolmogorov-Smirnov (KS) score against the uniform distribution is calculated on those  $p$ -values. The entire procedure is then repeated 100 times.

A second simulation is conducted for a graph with  $n = 20$  nodes, simulating  $m = 10,000$  events from a MEG model with interaction term only, corresponding to  $\lambda_{ij}(t) = A_{ij}\gamma_{ij}(t)$ , with  $r = 1$  and  $d = 5$ . A minor modification is made to the range of the uniform distributions for sampling some of the interaction term parameters:  $\gamma_{il}, \gamma'_{j\ell} \in (10^{-5}, 10^{-1})$ ,  $\nu_{il}, \nu'_{j\ell}, \theta_{il}, \theta'_{j\ell} \in (10^{-2}, 1)$ . Despite the simpler form of the intensity functions  $\lambda_{ij}(t)$ , the inferential task is more difficult than the previous simulation: more parameters must be estimated ( $2n \times 3d = 600$ ), and the expected number of connections per edge is only 105. The resulting boxplots of the KS test obtained for the two simulations are plotted in Figure 2.

As might be expected, the results of the first simulation, which corresponds to an easier estimation task, are slightly better than the second simulation. Both boxplots demonstrate that the algorithm is able to recover sensible estimates of the parameter values, resulting in small KS scores, corresponding to a good model fit.

### 4.2 Enron e-mail network

The Enron e-mail network collection is a record of e-mails exchanged between the employees of Enron Corporation before its bankruptcy. These data have already been demonstrated to be well-modelled as

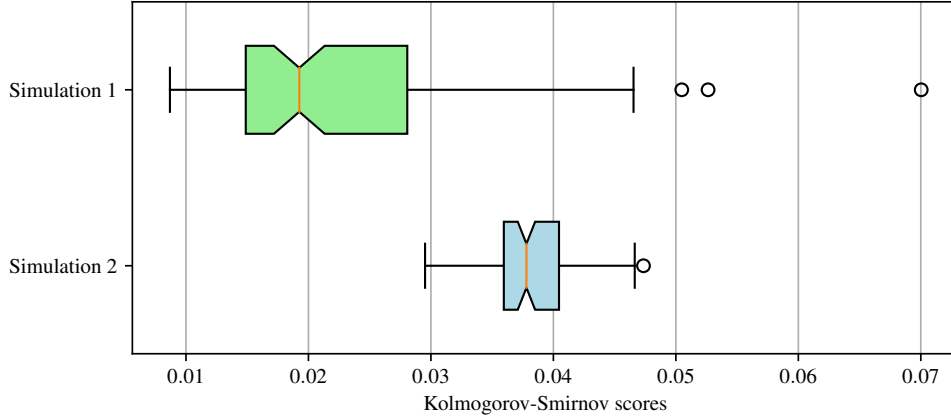


**Figure 2:** Boxplots of the Kolmogorov-Smirnov scores obtained for the two simulations described in Section 4.1.

self-exciting point processes by Fox et al. (2016). In this article, the version of these data<sup>1</sup> used in Priebe et al. (2005) is analysed, where e-mails recorded multiple times have been used only once, and e-mails with incorrectly recorded sent times (coded in the data with 9pm, 31 December 1979) have been removed. After such pre-processing, the e-mail data consist of 34,427 distinct triplets  $(x_k, y_k, t_k)$ , corresponding to messages exchanged between  $n = 184$  employees between November 1998 and June 2002, forming a total of 3,007 graph edges. Note that some of the emails are sent to multiple receivers, and only 18,031 unique event times are observed, implying that on average each e-mail is sent to approximately 1.90 nodes.

Because an e-mail can have multiple recipients, and because the event times are recorded to the nearest second, the likelihood (2.6) must be adapted slightly to handle tied arrival times. An approach used by Price-Williams and Heard (2020, Section 8.1) is followed, with the arrivals modelled by an analogous discrete time process: In particular, arrivals at time  $t$  are assumed to contribute to the intensities  $\lambda_{ij}(\cdot)$  from time  $t + dt$  onwards, where  $dt$  is the sampling interval, equal to one second in this example. The  $p$ -values of the process are approximated using (3.1), following Fox et al. (2016).

The model is trained on 30,704 e-mails sent before 1st December, 2001, and trained on the remaining 3,723 e-mails. In the training set, 2,720 edges are observed, and 811 in the test set, of which 287 are *not* observed in the training period. One of the advantages of the proposed methodology is the possibility to score events for such new links.

A range of MEG models are fitted to the training data, using different combinations of  $r$  and  $d$  for characterising main effects and interactions. A good configuration for the initial parameter values is obtained through utilising the quantities  $q_i = \frac{N_i(T)}{nT}$  and  $q'_j = \frac{N'_j(T)}{nT}$ , corresponding to the average rate of incoming and outgoing connections observed for each node. In particular, good results and convergence are obtained setting initial values  $\alpha_i = \mu_i = q_i$ ,  $\phi_i = 3q_i$ ,  $\beta_j = \mu'_j = q'_j$ , and  $\phi'_j = 3q'_j$ . For the interaction term, the initial values used to obtain the results are  $\gamma_{i\ell} = \gamma'_{j\ell} = \nu_{i\ell} = \nu'_{j\ell} = 10^{-4}$ , and  $\theta_{i\ell} = \theta'_{j\ell} = 5 \cdot 10^{-4}$ . If  $d > 1$ , then Gaussian noise with standard deviation  $2 \cdot 10^{-5}$  is added to the interaction parameters. In general, the algorithm is fairly robust to different initialisations if the scale of the parameters is similar to the choices above. The learning rate  $\eta$  is set to 0.1.

Three strategies are used for estimation of  $\tau_{ij}$ : (i) Using the MLE  $\hat{\tau}_{ij} = t_{\ell_{ij1}}$ ; (ii) Setting  $\tau_{ij} = 0$ ; (iii) Setting  $\tau_{ij} = 0$  if  $A_{ij} = 1$ , and  $\tau_{ij} = \infty$  if  $A_{ij} = 0$ . The MLE approach (i) has a drawback: the  $p$ -values (3.1) for the first observation on each edge are *always* 1. This implies that the KS scores are

<sup>1</sup>The data are freely available at <http://www.cis.jhu.edu/~parky/Enron/>.



**Table 1:** Training and test Kolmogorov-Smirnov scores on the Enron e-mail network for different configurations of the MEG model.

KS scores (train & test)		Main effects $\alpha_i(\cdot)$ and $\beta_j(\cdot)$ ↓								
$\tau_{ij}$ ↓	Interactions $\gamma_{ij}(\cdot)$ ↓	Absent		Poisson ( $r = 0$ )		Markov ( $r = 1$ )		Hawkes ( $r = \infty$ )		
$\tau_{ij} = t_{\ell_{ij1}}$ (MLE)	Absent	–	–	0.4530	0.4133	0.3678	0.3484	0.4443	0.3586	
	Poisson ( $r = 0$ )	$d = 1$	0.4252	0.4221	0.3946	0.4179	0.3434	0.3574	0.4255	0.3560
		$d = 5$	0.3490	0.3851	0.3498	0.3953	0.3165	0.3677	0.3491	0.3613
		$d = 10$	0.3339	0.3763	0.3347	0.3688	0.3112	0.3470	0.3376	0.3575
	Markov ( $r = 1$ )	$d = 1$	0.1662	0.2029	0.1491	0.1945	0.1305	0.1777	0.1702	0.1874
		$d = 5$	0.0916	0.1875	0.0910	0.1684	<b>0.0885</b>	<b>0.1628</b>	0.0916	0.1746
		$d = 10$	<b>0.0885</b>	0.1743	<b>0.0885</b>	0.1848	<b>0.0885</b>	0.1696	<b>0.0885</b>	0.1743
	Hawkes ( $r = \infty$ )	$d = 1$	0.2640	0.2755	0.2825	0.2887	0.2538	0.2637	0.2599	0.2871
		$d = 5$	0.2304	0.2904	0.2284	0.2760	0.2271	0.2774	0.2420	0.2981
		$d = 10$	0.2461	0.2923	0.2521	0.2865	0.2413	0.3091	0.2498	0.3129
	$\tau_{ij} = 0$	Absent	–	–	0.7678	0.7983	0.7456	0.7360	0.7058	0.6046
		Poisson ( $r = 0$ )	$d = 1$	0.7039	0.7926	0.6627	0.7753	0.6543	0.7148	0.7059
$d = 5$			0.5623	0.7059	0.5646	0.7206	0.5748	0.7008	0.7060	0.6053
$d = 10$			0.5354	0.6853	0.5332	0.6739	0.5725	0.6952	0.7060	0.6059
Markov ( $r = 1$ )		$d = 1$	0.3135	0.3324	0.3004	0.3326	0.3262	0.3240	0.2027	0.1999
		$d = 5$	0.0760	0.1664	0.0825	0.1584	0.0855	0.1782	0.0495	<b>0.0924</b>
		$d = 10$	0.0775	0.1649	0.0793	0.1546	0.0816	0.1606	<b>0.0402</b>	0.0971
Hawkes ( $r = \infty$ )		$d = 1$	0.2871	0.2486	0.2333	0.2449	0.2485	0.2379	0.1749	0.1991
		$d = 5$	0.1939	0.2167	0.1885	0.2246	0.2010	0.2137	0.1467	0.1994
		$d = 10$	0.2029	0.2395	0.2158	0.2470	0.2207	0.2339	0.1606	0.1943
$\tau_{ij} = \begin{cases} 0, & A_{ij} = 1 \\ \infty, & A_{ij} = 0 \end{cases}$		Absent	–	–	0.5590	0.5941	0.4112	0.3667	0.4593	0.2758
		Poisson ( $r = 0$ )	$d = 1$	0.5158	0.6038	0.4812	0.5864	0.3742	0.3602	0.4197
	$d = 5$		0.4269	0.5516	0.4309	0.5641	0.3553	0.3598	0.3938	0.2803
	$d = 10$		0.4035	0.5413	0.4084	0.5565	0.3430	0.3537	0.3659	0.2810
	Markov ( $r = 1$ )	$d = 1$	0.1950	0.2115	0.1600	0.2017	0.1504	0.1422	0.1309	0.1445
		$d = 5$	0.0709	0.1222	0.0746	0.1008	0.0696	0.0917	<b>0.0152</b>	0.0848
		$d = 10$	0.0619	0.1029	0.0627	0.1079	0.0634	0.0836	0.0213	<b>0.0800</b>
	Hawkes ( $r = \infty$ )	$d = 1$	0.1870	0.2084	0.1816	0.2049	0.1783	0.1747	0.1719	0.1879
		$d = 5$	0.1377	0.1805	0.1374	0.1840	0.1391	0.1642	0.1553	0.2154
		$d = 10$	0.1556	0.2023	0.1588	0.2046	0.1546	0.1863	0.1640	0.2082

bounded below by  $2720/30704 \approx 0.0885$  for the training set and  $287/3723 \approx 0.0770$  for the test set.

The KS scores obtained on the training and test sets after fitting different MEG models are reported in Table 1. The best performance (KS score 0.0152) is achieved when a Markov process is used for the interaction term, with  $d = 5$  or  $d = 10$ , combined with a Hawkes process for the main effects, setting  $\tau_{ij}$  using option (iii). The same model achieves the best performance when alternative strategies for estimation of  $\tau_{ij}$  are used. If  $\tau_{ij}$  is set to its MLE (i), then the lower bound for the KS score on the training set is attained. In general, setting  $\tau_{ij}$  using option (iii) seems to outperform competing strategies for estimation of  $\tau_{ij}$  in terms of KS scores. More importantly, overall the results demonstrate that the interaction term plays a key role in obtaining a good fit on the observed event times.

The results on the training set can also be compared to alternative node-based models from the literature. For example, Fox et al. (2016) propose the following node-specific intensity function for sending

e-mails:

$$\lambda_i(t) = \alpha_i + \sum_{k=1}^{N'_i(t)} \mu_i \exp\{-(\mu_i + \phi_i)(t - t'_{ik})\}, \quad (4.1)$$

where the intensity jumps according to the event times of the *received* e-mails (*cf.* (2.2) and (2.3)). Despite the present article using a slightly different number of e-mails, the Kolmogorov-Smirnov score obtained on the training data using (4.1) is 0.2806, which corresponds almost exactly to the result in Fox et al. (2016), demonstrating that the MEG appears to have superior performance for the Enron network. The parameters of (4.1) are estimated by direct optimisation using the Nelder-Mead method on the negative log-likelihood function for each source node. Nearly identical results to Fox et al. (2016) are also obtained from fitting an independent Poisson processes  $\lambda_i(t) = \alpha_i$  on each source node, with KS score 0.4088. Finally, independent Hawkes process models of the form (1.1) are also fitted to each source node, obtaining a KS score of 0.2499 which is significantly outperformed by the best configuration of the MEG model. Since the MEG model KS score outperforms the value obtained using (4.1), it could be inferred that users tend to respond to multiple e-mails in sessions, and not necessarily immediately after an individual e-mail is received.

### 4.3 Imperial College London NetFlow data

Many enterprises routinely collect network flow (NetFlow) data, representing summaries of connections between internet protocol (IP) addresses (see, for example, Hofstede et al., 2014). A bipartite dynamic network has been constructed from a subset of such data collected at Imperial College London (ICL). The network consists of 1,951,067 arrival times recorded to the nearest millisecond, observed between 20th January 2020, and 9th February 2020, recorded from  $n_1 = 173$  clients hosted within the Department of Mathematics at ICL, connecting to  $n_2 = 6,083$  internet servers connecting on ports 80 and 443 (corresponding to unencrypted and encrypted web traffic), forming a total of 156,186 unique edges. The periodic and automated activity has been filtered by considering only edges such that the percentage of arrival times observed between 7am and 12am is larger than 99%, corresponding to the Department of Mathematics building opening hours. To learn connectivity patterns, the MEG model is trained on the first two weeks of data, corresponding to 1,299,372 events, and tested on 651,695 events observed in the final week. The number of unique edges observed in the training period is 115,600, and 70,408 in the test set; only 29,822 edges are observed in both time windows, which implies that 40,586 new edges are observed in the test set.

As discussed in Section 1, computer network data are observed in bursts and exhibit periodic behaviour. Figure 3 gives an example of the connections from two of the clients to the ICL Virtual Learning Environment (VLE) server. Each session begins at an hour consistent with human behaviour, while the frequency of subsequent connections within each session is likely to be due to automated activity and page refreshing.

The models have been initialised using a similar initialisation scheme to Section 4.2, with learning rate  $\eta = 0.5$ . In particular, setting  $q_i = \frac{N_i(T)}{n_1 T}$  and  $q'_j = \frac{N'_j(T)}{n_2 T}$ , the chosen initial values are  $\alpha_i = \mu_i = q_i$ ,  $\phi_i = 3q_i$ ,  $\beta_j = \mu'_j = q'_j$ , and  $\phi'_j = 3q'_j$ ,  $\gamma_{i\ell} = (q_i)^{1/2}$ ,  $\gamma'_{j\ell} = (q'_j)^{1/2}$ ,  $\nu_{i\ell} = \nu'_{j\ell} = 10^{-4}$ , and  $\theta_{i\ell} = \theta'_{j\ell} = 5 \cdot 10^{-4}$ . As before, Gaussian noise is added to the interaction parameters if  $d > 1$ .

The likelihood for the Hawkes process is highly multimodal, and more sensitive to the initial values of the parameters than the Markov process with  $r = 1$ . Therefore, the parameters for the Hawkes process models are initialised with the optimal values obtained from the corresponding Markov process models, which seems to lead to fast convergence. The Kolmogorov-Smirnov scores calculated on the training and

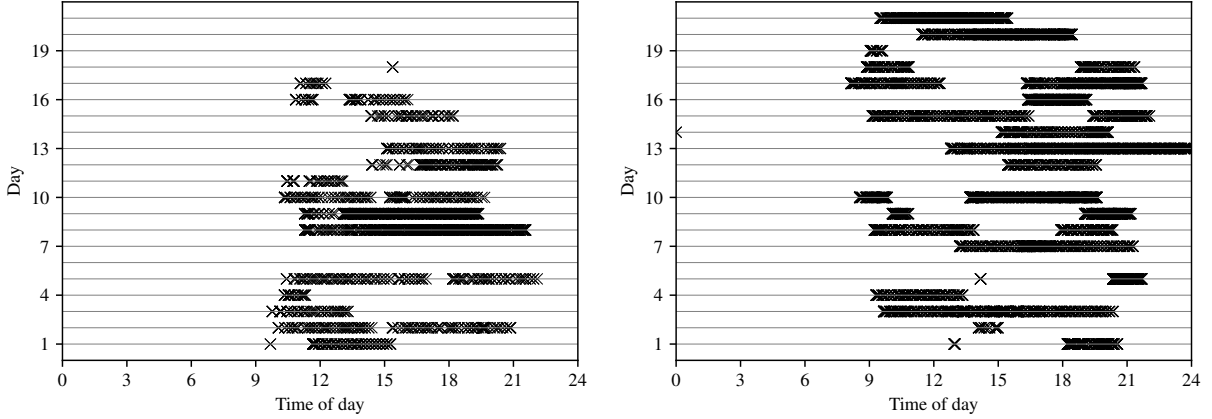


Figure 3: Connections to the ICL Virtual Learning Environment from two clients.

Table 2: Kolmogorov-Smirnov scores on the ICL NetFlow data for different configurations of the MEG model.

KS scores (train & test)		Main effects $\alpha_i(\cdot)$ and $\beta_j(\cdot)$ ↓							
		Interactions $\gamma_{ij}(\cdot)$ ↓		Absent		Poisson ( $r = 0$ )		Markov ( $r = 1$ )	
Absent		–		0.7351 0.7148		0.6678 0.6489		0.7312 0.6950	
Poisson ( $r = 0$ )	$d = 1$	0.7328 0.7157		0.7325 0.7150		0.6672 0.6480		0.7316 0.6960	
	$d = 5$	0.7295 0.7167		0.7313 0.7123		0.6673 0.6487		0.7275 0.6967	
	$d = 10$	0.7260 0.7174		0.7289 0.7140		0.6680 0.6493		0.7270 0.6969	
Markov ( $r = 1$ )	$d = 1$	0.2194 0.1723		0.2242 0.1657		0.2038 0.1440		0.1645 0.1281	
	$d = 5$	0.1024 0.1080		0.0896 0.0805		<b>0.0728 0.0738</b>		0.1041 0.0899	
	$d = 10$	0.0843 0.0764		0.0871 0.0761		0.0850 0.0843		0.1100 0.0883	
Hawkes ( $r = \infty$ )	$d = 1$	0.1080 0.0802		0.0747 0.1182		0.1082 0.0794		0.0884 0.1262	
	$d = 5$	0.1576 0.1819		0.1532 0.2126		0.1677 0.2143		0.2307 0.2383	
	$d = 10$	0.1584 0.1935		0.1546 0.2112		0.1619 0.2206		0.2388 0.2503	

test set arrival times for different MEG models are reported in Table 2. The parameter  $\tau_{ij}$  is set according to option (iii) from Section 4.2, which was observed to have the best performance on the Enron data.

The best performance (KS score 0.0728) is achieved by a Markov process with  $r = 1$  for both the main effects and interactions, and latent dimensionality  $d = 5$  for the parameters of the interaction term. Corresponding Q-Q plots for some of the models are plotted in Figure 4. Overall, the table and plots demonstrate that correctly modelling the arrival times requires inclusion within the model of an interaction term with a self-exciting component. Because of the extremely bursty behaviour of NetFlow arrival times, the Markov process model for main effects and interactions intuitively appears to be a suitable choice.

Finally, for the best performing model the corresponding KS scores are calculated individually for each edge, and plotted in Figure 5 as a function of the number of connections on the edge. Clearly, the model has a better performance at scoring arrival times on more active edges.

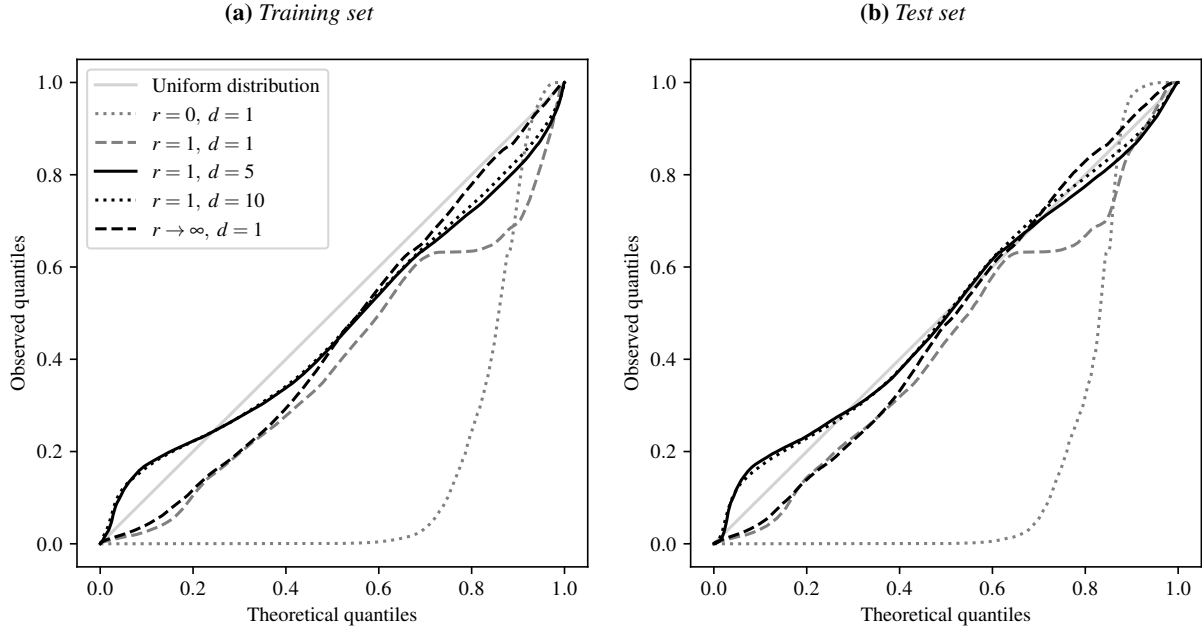


**Figure 4:**  $Q-Q$  plots for the training and test  $p$ -values obtained from different MEG models, with main effects  $\alpha_i(t)$  and  $\beta_j(t)$  with  $r = 1$ , and different parameters for the interaction term  $\gamma_{ij}(t)$ , specified in the legend.

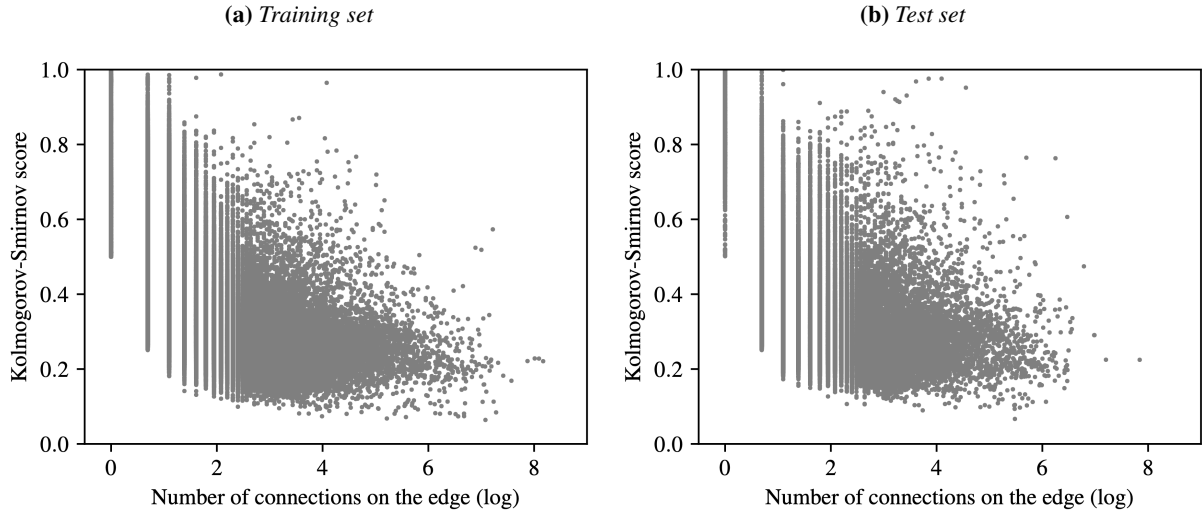


**Figure 5:** Scatterplot of the Kolmogorov-Smirnov scores, calculated for each edge, versus the logarithm of the total number of connections on the edge, for the best performing model in Table 2.

## 5 Conclusion

The mutually-exciting graph (MEG), a novel network-wide model for point processes with dyadic marks has been proposed. MEG uses mutually exciting point processes to model intensity functions, and borrows ideas from latent space models to infer relationships between the nodes. Edge-specific intensities are obtained only via node-specific parameters, which is useful for large and sparse graphs. Importantly, the proposed model is able to predict events observed on *new* edges. Inference is performed via maximum

likelihood estimation, optimised numerically using modern gradient ascent algorithms. The model has been tested on simulated data and on two data sources related to computer networking: ICL NetFlow data and the Enron e-mail network. MEG appears to have excellent goodness-of-fit on training and testing data, resulting in low Kolmogorov-Smirnov scores even on very large and heterogeneous data like network flows. Furthermore, for the Enron e-mail network, MEG greatly outperforms results previously obtained in the literature on the same data. The model has been specifically motivated by cyber-security applications, where scoring observations on new links is particularly important for network security. Within this context, MEG might be used to complement existing techniques for modelling sequences of edges on dynamic networks (Sanna Passino and Heard, 2019), providing a network-wide method for scoring arrival times.

## Code

The *python* code to reproduce the results in this paper, and a *bash* script to obtain the Enron e-mail network data, are available in the *GitHub* repository [fraspas/meg](https://github.com/fraspas/meg).

## Acknowledgements

This work is funded by the Microsoft Security AI research grant “*Understanding the enterprise: Host-based event prediction for automatic defence in cyber-security*”. The authors thank Dr Melissa J. M. Turcotte for helpful discussions and comments.

## References

- Athreya, A., Fishkind, D. E., Tang, M., Priebe, C. E., Park, Y., Vogelstein, J. T., Levin, K., Lyzinski, V., Qin, Y. and Sussman, D. L. (2018) Statistical inference on random dot product graphs: a survey. *Journal of Machine Learning Research*, **18**, 1–92.
- Bowsher, C. G. (2007) Modelling security market events in continuous time: Intensity based, multivariate point process models. *Journal of Econometrics*, **141**, 876 – 912.
- Brown, E., Barbieri, R., Ventura, V., Kass, R. and Frank, L. (2002) The time-rescaling theorem and its application to neural spike train data analysis. *Neural computation*, **14**, 325–346.
- Chen, F. and Tan, W. H. (2018) Marked self-exciting point process modelling of information diffusion on Twitter. *Annals of Applied Statistics*, **12**, 2175–2196.
- Daley, D. and Vere-Jones, D. (2002) *An Introduction to the Theory of Point Processes – Volume I: Elementary Theory and Methods*. Probability and Its Applications. Springer.
- Durante, D. and Dunson, D. B. (2016) Locally adaptive dynamic networks. *Annals of Applied Statistics*, **10**, 2203–2232.
- Eichler, M., Dahlhaus, R. and Dueck, J. (2017) Graphical modeling for multivariate Hawkes processes with nonparametric link functions. *Journal of Time Series Analysis*, **38**, 225–242.
- Etesami, J., Kiyavash, N., Zhang, K. and Singhal, K. (2016) Learning network of multivariate Hawkes processes: A time series approach. In *Proceedings of the Thirty-Second Conference on Uncertainty in Artificial Intelligence*, UAI’16, 162–171. Arlington, Virginia, USA: AUAI Press.

- Fox, E., Short, M., Schoenberg, F., Coronges, K. and Bertozzi, A. (2016) Modeling e-mail networks and inferring leadership using self-exciting point processes. *Journal of the American Statistical Association*, **111**, 564–584.
- Hawkes, A. (1971) Spectra of some self-exciting and mutually exciting point processes. *Biometrika*, **58**, 83–90.
- Heard, N. A., Rubin-Delanchy, P. T. G. and Lawson, D. J. (2014) Filtering automated polling traffic in computer network flow data. *Proceedings - 2014 IEEE Joint Intelligence and Security Informatics Conference, JISIC 2014*, 268–271.
- Hoff, P. D. (2018) Additive and multiplicative effects network models. *arXiv e-prints*.
- Hoff, P. D., Raftery, A. E. and Handcock, M. S. (2002) Latent space approaches to social network analysis. *Journal of the American Statistical Association*, **97**, 1090–1098.
- Hofstede, R., Čeleda, P., Trammell, B., Drago, I., Sadre, R., Sperotto, A. and Pras, A. (2014) Flow monitoring explained: From packet capture to data analysis with NetFlow and IPFIX. *IEEE Communications Surveys Tutorials*, **16**, 2037–2064.
- Kingma, D. P. and Ba, J. (2015) Adam: a method for stochastic optimization. In *3rd International Conference on Learning Representations, ICLR* (eds. Y. Bengio and Y. LeCun). San Diego, CA, USA.
- Krivitsky, P. N. and Handcock, M. S. (2014) A separable model for dynamic networks. *Journal of the Royal Statistical Society: Series B*, **76**, 29–46.
- Linderman, S. W. and Adams, R. P. (2014) Discovering latent network structure in point process data. In *Proceedings of the 31st International Conference on International Conference on Machine Learning - Volume 32, ICML'14*, II–1413–II–1421.
- Metelli, S. and Heard, N. A. (2019) On Bayesian new edge prediction and anomaly detection in computer networks. *Annals of Applied Statistics*, **13**, 2586–2610.
- Mohler, G. O., Short, M. B., Brantingham, P. J., Schoenberg, F. P. and Tita, G. E. (2011) Self-exciting point process modeling of crime. *Journal of the American Statistical Association*, **106**, 100–108.
- Neil, J., Hash, C., Brugh, A., Fisk, M. and Storlie, C. B. (2013) Scan statistics for the online detection of locally anomalous subgraphs. *Technometrics*, **55**, 403–414.
- Ogata, Y. (1978) The asymptotic behaviour of maximum likelihood estimators for stationary point processes. *Annals of the Institute of Statistical Mathematics*, **30**, 243–261.
- Ogata, Y. (1981) On Lewis' simulation method for point processes. *IEEE Transactions on Information Theory*, **27**, 23–31.
- Ogata, Y. (1988) Statistical models for earthquake occurrences and residual analysis for point processes. *Journal of the American Statistical Association*, **83**, 9–27.
- Ozaki, T. (1979) Maximum likelihood estimation of Hawkes' self-exciting point processes. *Annals of the Institute of Statistical Mathematics*, **31**, 145–155.



- Perry, P. and Wolfe, P. (2013) Point process modelling for directed interaction networks. *Journal of the Royal Statistical Society: Series B (Statistical Methodology)*, **75**, 821–849.
- Price-Williams, M. and Heard, N. A. (2020) Nonparametric self-exciting models for computer network traffic. *Statistics and Computing*, **30**, 209–220.
- Priebe, C. E., Conroy, J. M., Marchette, D. J. and Park, Y. (2005) Scan statistics on Enron graphs. *Computational & Mathematical Organization Theory*, **11**, 229–247.
- Ruder, S. (2016) An overview of gradient descent optimization algorithms. *arXiv e-prints*.
- Sanna Passino, F. and Heard, N. A. (2019) Modelling dynamic network evolution as a Pitman-Yor process. *Foundations of Data Science*, **1**, 293–306.
- Sarkar, P. and Moore, A. W. (2006) Dynamic social network analysis using latent space models. In *Advances in Neural Information Processing Systems 18*, 1145–1152.
- Sewell, D. K. and Chen, Y. (2015) Latent space models for dynamic networks. *Journal of the American Statistical Association*, **110**, 1646–1657.
- Stomakhin, A., Short, M. B. and Bertozzi, A. L. (2011) Reconstruction of missing data in social networks based on temporal patterns of interactions. *Inverse Problems*, **27**.
- Zhao, Q., Erdogdu, M. A., He, H. Y., Rajaraman, A. and Leskovec, J. (2015) Seismic: A self-exciting point process model for predicting tweet popularity. In *Proceedings of the 21th ACM SIGKDD International Conference on Knowledge Discovery and Data Mining*, KDD '15, 1513–1522.

## A Appendix

### A.1 Calculation of the log-likelihood in MEG models

According to the choice of the excitation function and the parameter  $r$ , the log-likelihood (2.6) takes different forms. Here, examples are given for MEG models with  $d = 1$ ,  $r = 1$  or  $r = \infty$ , with scaled exponential excitation functions. For simplicity, since  $d = 1$ , the second subscript  $\ell$  is dropped from the triplets  $(\gamma_{i\ell}, \nu_{i\ell}, \theta_{i\ell})$  and  $(\gamma'_{j\ell}, \nu'_{j\ell}, \theta'_{j\ell})$ . Assume two sequences of arrival times  $t_1 < \dots < t_{n_i}$  involving  $i$  as source node, and  $t'_1 < \dots < t'_{n'_j}$  such that  $j$  is the destination of the connection. Within the two sequences of arrival times  $t_1, \dots, t_{n_i}$  and  $t'_1, \dots, t'_{n'_j}$ , assume that a subset of  $n_{ij}$  events, with  $n_{ij} \leq \min\{n_i, n'_j\}$ , is observed on the edge  $(i, j)$ . Denote the indices of such events as  $\ell_1, \dots, \ell_{n_{ij}}$  and  $\ell'_1, \dots, \ell'_{n_{ij}}$ , such that  $t_{\ell_k} = t'_{\ell'_k}$ . Define  $\bar{t}_k = \max\{t_h : t_h < t_{\ell_k}\}$  and  $\bar{t}'_k = \max\{t'_h : t'_h < t'_{\ell'_k}\}$ . For the edge  $(i, j)$ , assuming  $r = 1$ , the first part of the log-likelihood (2.6) is:

$$\sum_{k=1}^{n_{ij}} \log \lambda_{ij}(t_{\ell_k}) = \sum_{k=1}^{n_{ij}} \log \left\{ \alpha_i + \mu_i e^{-(\mu_i + \phi_i)(t_{\ell_k} - \bar{t}_k)} + \beta_j + \mu'_j e^{-(\mu'_j + \phi'_j)(t'_{\ell'_k} - \bar{t}'_k)} + \gamma_i \gamma'_j + \nu_i \nu'_j e^{-(\nu_i + \theta_i)(\nu'_j + \theta'_j)(t_{\ell_k} - t_{\ell_{k-1}})} \right\}. \quad (\text{A.1})$$

For Hawkes process models, the main computational burden associated with the calculation of the likelihood is the double summation arising in the first term of (2.6) when  $r = \infty$ . The term in the first sum in (2.6) can be written as:

$$\sum_{k=1}^{n_{ij}} \log \lambda_{ij}(t_{\ell_k}) = \sum_{k=1}^{n_{ij}} \log \left\{ \alpha_i + \mu_i \sum_{h=1}^{\ell_k-1} e^{-(\mu_i + \phi_i)(t_{\ell_k} - t_h)} + \beta_j + \mu'_j \sum_{h=1}^{\ell'_k-1} e^{-(\mu'_j + \phi'_j)(t'_{\ell'_k} - t'_h)} + \gamma_i \gamma'_j + \nu_i \nu'_j \sum_{h=1}^{k-1} e^{-(\nu_i + \theta_i)(\nu'_j + \theta'_j)(t_{\ell_k} - t_{\ell_h})} \right\}. \quad (\text{A.2})$$

Using a technique similar to the method proposed in Ogata (1978), it is possible to calculate (A.2) in linear time using a recursive formulation of the inner summations. For  $k \in \{2, \dots, n_{ij}\}$ , define  $\psi_{ij}(k)$ ,  $\psi'_{ij}(k)$  and  $\tilde{\psi}_{ij}(k)$  as follows:

$$\begin{aligned} \psi_{ij}(k) &= \sum_{h=1}^{\ell_k-1} e^{-(\mu_i + \phi_i)(t_{\ell_k} - t_h)}, & \psi'_{ij}(k) &= \sum_{h=1}^{\ell'_k-1} e^{-(\mu'_j + \phi'_j)(t'_{\ell'_k} - t'_h)}, \\ \tilde{\psi}_{ij}(k) &= \sum_{h=1}^{k-1} e^{-(\nu_i + \theta_i)(\nu'_j + \theta'_j)(t_{\ell_k} - t_{\ell_h})}, \end{aligned} \quad (\text{A.3})$$

assuming the initial conditions  $\tilde{\psi}_{ij}(1) = 0$  and

$$\psi_{ij}(1) = \sum_{h=1}^{\ell_1-1} e^{-(\mu_i + \phi_i)(t_{\ell_1} - t_h)}, \quad \psi'_{ij}(1) = \sum_{h=1}^{\ell'_1-1} e^{-(\mu'_j + \phi'_j)(t'_{\ell'_1} - t'_h)}.$$

Note that the subscript  $(i, j)$  for  $\psi_{ij}(k)$  and  $\psi'_{ij}(k)$  is required since  $\ell_k$  and  $\ell'_k$  are edge-specific values, and represent a short hand notation for  $\ell_{ijk}$  and  $\ell'_{ijk}$ . Using (A.3), the first term (A.2) of the likelihood becomes:

$$\sum_{k=1}^{n_{ij}} \log \lambda_{ij}(t_{\ell_k}) = \sum_{k=1}^{n_{ij}} \log \left\{ \alpha_i + \beta_j + \gamma_i \gamma'_j + \mu_i \psi_{ij}(k) + \mu'_j \psi'_{ij}(k) + \nu_i \nu'_j \tilde{\psi}_{ij}(k) \right\}.$$

**Proposition 1.** *The terms  $\psi_{ij}(k)$ ,  $\psi'_{ij}(k)$  and  $\tilde{\psi}_{ij}(k)$  can be written recursively as follows:*

$$\begin{aligned} \psi_{ij}(k) &= e^{-(\mu_i + \phi_i)(t_{\ell_k} - t_{\ell_{k-1}})} [1 + \psi_{ij}(k-1)] + \sum_{h=\ell_{k-1}+1}^{\ell_k-1} e^{-(\mu_i + \phi_i)(t_{\ell_k} - t_h)}, \\ \psi'_{ij}(k) &= e^{-(\mu'_j + \phi'_j)(t'_{\ell'_k} - t'_{\ell'_{k-1}})} [1 + \psi'_{ij}(k-1)] + \sum_{h=\ell'_{k-1}+1}^{\ell'_k-1} e^{-(\mu'_j + \phi'_j)(t'_{\ell'_k} - t'_h)}, \\ \tilde{\psi}_{ij}(k) &= e^{-(\nu_i + \theta_i)(\nu'_j + \theta'_j)(t_{\ell_k} - t_{\ell_{k-1}})} [1 + \tilde{\psi}_{ij}(k-1)]. \end{aligned} \quad (\text{A.4})$$

*Proof.* The result is proved here for  $\psi_{ij}(k)$ .

$$\begin{aligned}
 \psi_{ij}(k) &= \sum_{h=1}^{\ell_k-1} e^{-(\mu_i+\phi_i)(t_{\ell_k}-t_h)} = \sum_{h=1}^{\ell_k-1} e^{-(\mu_i+\phi_i)(t_{\ell_k}-t_h)} + \sum_{h=\ell_{k-1}+1}^{\ell_k-1} e^{-(\mu_i+\phi_i)(t_{\ell_k}-t_h)} \\
 &= e^{-(\mu_i+\phi_i)(t_{\ell_k}-t_{\ell_{k-1}})+(\mu_i+\phi_i)(t_{\ell_k}-t_{\ell_{k-1}})} \sum_{h=1}^{\ell_k-1} e^{-(\mu_i+\phi_i)(t_{\ell_k}-t_h)} + \sum_{h=\ell_{k-1}+1}^{\ell_k-1} e^{-(\mu_i+\phi_i)(t_{\ell_k}-t_h)} \\
 &= e^{-(\mu_i+\phi_i)(t_{\ell_k}-t_{\ell_{k-1}})} \sum_{h=1}^{\ell_k-1} e^{-(\mu_i+\phi_i)(t_{\ell_{k-1}}-t_h)} + \sum_{h=\ell_{k-1}+1}^{\ell_k-1} e^{-(\mu_i+\phi_i)(t_{\ell_k}-t_h)} \\
 &= e^{-(\mu_i+\phi_i)(t_{\ell_k}-t_{\ell_{k-1}})} \left[ 1 + \sum_{h=1}^{\ell_{k-1}-1} e^{-(\mu_i+\phi_i)(t_{\ell_{k-1}}-t_h)} \right] + \sum_{h=\ell_{k-1}+1}^{\ell_k-1} e^{-(\mu_i+\phi_i)(t_{\ell_k}-t_h)},
 \end{aligned}$$

which, using the definition of  $\psi_{ij}(k-1)$ , gives the result (A.4). The proof for  $\psi'_{ij}(k)$  follows similar steps, but the summation is splitted at  $\ell'_{k-1}$ , and the first summation is multiplied and divided by  $e^{-(\mu'_j+\phi'_j)(t'_{\ell'_k}-t'_{\ell'_{k-1}})}$ . For  $\tilde{\psi}_{ij}(k)$ , the decomposition is analogous to standard Hawkes processes.  $\square$

The second part of the log-likelihood (2.6) is equivalent to  $\Lambda_{ij}(T)$  and follows from integration of  $\lambda_{ij}(t)$  over the observation period. For  $r = 1$ :

$$\begin{aligned}
 \int_0^T \lambda_{ij}(t) dt &= (\alpha_i + \beta_j + \gamma_i \gamma'_j)(T - \tau_{ij}) - \frac{\nu_i \nu'_j}{(\nu_i + \theta_i)(\nu'_j + \theta'_j)} \sum_{k=1}^{n_{ij}} \left[ e^{-(\nu_i + \theta_i)(\nu'_j + \theta'_j)(t_{\ell_{k+1}} - t_{\ell_k})} - 1 \right] \\
 &- \frac{\mu_i}{\mu_i + \phi_i} \sum_{k=1}^{n_i} \mathbb{1}_{[\tau_{ij}, \infty)}(t_k) \left[ e^{-(\mu_i + \phi_i)(t_{k+1} - t_k)} - 1 \right] - \frac{\mu'_j}{\mu'_j + \phi'_j} \sum_{k=1}^{n'_j} \mathbb{1}_{[\tau_{ij}, \infty)}(t'_k) \left[ e^{-(\mu'_j + \phi'_j)(t'_{k+1} - t'_k)} - 1 \right] \\
 &- \frac{\mu_i}{\mu_i + \phi_i} \left[ e^{-(\mu_i + \phi_i)(\min\{t_h: t_h \geq \tau_{ij}\} - \max\{t_h: t_h \leq \tau_{ij}\})} - e^{-(\mu_i + \phi_i)(\tau_{ij} - \max\{t_h: t_h \leq \tau_{ij}\})} \right] \\
 &- \frac{\mu'_j}{\mu'_j + \phi'_j} \left[ e^{-(\mu'_j + \phi'_j)(\min\{t'_h: t'_h \geq \tau_{ij}\} - \max\{t'_h: t'_h \leq \tau_{ij}\})} - e^{-(\mu'_j + \phi'_j)(\tau_{ij} - \max\{t'_h: t'_h \leq \tau_{ij}\})} \right], \tag{A.5}
 \end{aligned}$$

where  $t_{n_i+1} = t'_{n'_j+1} = t_{\ell_{n_{ij}+1}} = T$ . Similarly, for  $r = \infty$  and  $\mathbb{1}_{[\tau_{ij}, \infty)}(T) = 1$ :

$$\begin{aligned}
 \int_0^T \lambda_{ij}(t) dt &= (\alpha_i + \beta_j + \gamma_i \gamma'_j)(T - \tau_{ij}) \tag{A.6} \\
 &- \frac{\mu_i}{\mu_i + \phi_i} \sum_{k=1}^{n_i} \left[ e^{-(\mu_i + \phi_i)(T - t_k)} - e^{-(\mu_i + \phi_i) \max\{\tau_{ij} - t_k, 0\}} \right] \\
 &- \frac{\mu'_j}{\mu'_j + \phi'_j} \sum_{k=1}^{n'_j} \left[ e^{-(\mu'_j + \phi'_j)(T - t'_k)} - e^{-(\mu'_j + \phi'_j) \max\{\tau_{ij} - t'_k, 0\}} \right] \\
 &- \frac{\nu_i \nu'_j}{(\nu_i + \theta_i)(\nu'_j + \theta'_j)} \sum_{k=1}^{n_{ij}} \left[ e^{-(\nu_i + \theta_i)(\nu'_j + \theta'_j)(T - t_{\ell_k})} - 1 \right].
 \end{aligned}$$

Note that (A.5) and (A.6) are monotonically decreasing functions in  $\tau_{ij}$  for any choice of the remaining parameters, with constraint  $\tau_{ij} < t_{\ell_{ij1}}$ , where  $t_{\ell_{ij1}}$  is the first arrival time on the edge  $(i, j)$ . Furthermore,  $\tau_{ij}$  does not explicitly appear in the first part of the likelihood, cf. (A.1) and (A.2). Therefore, using (2.6), the maximum likelihood estimate for  $\tau_{ij}$  is simply  $\hat{\tau}_{ij} = t_{\ell_{ij1}}$  if at least one event is observed on the edge, and  $\hat{\tau}_{ij} = \infty$  otherwise. If  $\tau_{ij}$  is set to its MLE, then the last two lines of (A.5) cancel out.

For the  $p$ -values in (3.1), for  $r = \infty$ , the difference between the compensators is calculated sequentially at the observed times  $t_1, \dots, t_{n_{ij}}$  using  $\psi_{ij}(k)$ ,  $\psi'_{ij}(k)$  and  $\tilde{\psi}_{ij}(k)$ :

$$\begin{aligned} \Lambda_{ij}(t_k) - \Lambda_{ij}(t_{k-1}) &= (\alpha_i + \beta_j + \gamma_i \gamma'_j)(t_k - t_{k-1}) \\ &\quad - \frac{\mu_i}{\mu_i + \phi_i} [\psi_{ij}(k) - N_i(t_k) - \psi_{ij}(k-1) + N_i(t_{k-1})] \\ &\quad - \frac{\mu'_j}{\mu'_j + \phi'_j} [\psi'_{ij}(k) - N'_j(t_k) - \psi'_{ij}(k-1) + N'_j(t_{k-1})] \\ &\quad - \frac{\nu_i \nu'_j}{(\nu_i + \theta_i)(\nu'_j + \theta'_j)} \left[ \tilde{\psi}_{ij}(k) - N_{ij}(t_k) - \tilde{\psi}_{ij}(k-1) + N_{ij}(t_{k-1}) \right]. \end{aligned}$$

An expression similar to (A.5) can be used for  $\Lambda_{ij}(t_k) - \Lambda_{ij}(t_{k-1})$  when  $r = 1$ .

## A.2 Calculation of the gradient for $r = \infty$

In the derivations of the gradient, the following notation is used:

$$\zeta_{ij}(k) = \alpha_i + \beta_j + \gamma_i \gamma'_j + \mu_i \psi_{ij}(k) + \mu'_j \psi'_{ij}(k) + \nu_i \nu'_j \tilde{\psi}_{ij}(k).$$

The partial derivative of  $\log L(\mathcal{H}_T | \Psi)$  with respect to  $\alpha_i$  and  $\gamma_i$  takes the following form:

$$\begin{aligned} \frac{\partial}{\partial \alpha_i} \log L(\mathcal{H}_T | \Psi) &= \sum_{j=1}^n \mathbb{1}_{[\tau_{ij}, \infty)}(T) \left[ -(T - \tau_{ij}) + \sum_{k=1}^{n_{ij}} \zeta_{ij}(k)^{-1} \right], \\ \frac{\partial}{\partial \gamma_i} \log L(\mathcal{H}_T | \Psi) &= \sum_{j=1}^n \gamma'_j \mathbb{1}_{[\tau_{ij}, \infty)}(T) \left[ -(T - \tau_{ij}) + \sum_{k=1}^{n_{ij}} \zeta_{ij}(k)^{-1} \right]. \end{aligned}$$

Similar equations can be derived for the partial derivatives with respect to  $\beta_j$  and  $\gamma'_j$ .

The calculations of the partial derivatives with respect to the parameters  $\mu_i$ ,  $\phi_i$ ,  $\mu'_j$  and  $\phi'_j$  use the recursive structure defined in the previous section, since the expressions  $\psi_{ij}(k)$  and  $\psi'_{ij}(k)$  are functions of  $(\mu_i, \phi_i)$  and  $(\mu'_j, \phi'_j)$  respectively. For  $\mu_i$  and  $\phi_i$ :

$$\begin{aligned} \frac{\partial}{\partial \mu_i} \log L(\mathcal{H}_T | \Psi) &= \frac{1}{\mu_i + \phi_i} \sum_{j=1}^n \mathbb{1}_{[\tau_{ij}, \infty)}(T) \sum_{k=1}^{n_{ij}} \left\{ \frac{\phi_i}{\mu_i + \phi_i} \left[ e^{-(\mu_i + \phi_i)(T-t_k)} - e^{-(\mu_i + \phi_i) \max\{\tau_{ij}-t_k, 0\}} \right] \right. \\ &\quad \left. - \mu_i \left[ (T - t_k) e^{-(\mu_i + \phi_i)(T-t_k)} - \max\{\tau_{ij} - t_k, 0\} e^{-(\mu_i + \phi_i) \max\{\tau_{ij}-t_k, 0\}} \right] \right\} \\ &\quad + \sum_{j=1}^n \mathbb{1}_{[\tau_{ij}, \infty)}(T) \sum_{k=1}^{n_{ij}} \frac{1}{\zeta_{ij}(k)} \left[ \psi_{ij}(k) + \mu_i \frac{\partial}{\partial \mu_i} \psi_{ij}(k) \right], \end{aligned}$$

$$\begin{aligned} \frac{\partial}{\partial \phi_i} \log L(\mathcal{H}_T | \Psi) &= - \frac{\mu_i}{\mu_i + \phi_i} \sum_{j=1}^n \mathbb{1}_{[\tau_{ij}, \infty)}(T) \sum_{k=1}^{n_{ij}} \left\{ \frac{1}{\mu_i + \phi_i} \left[ e^{-(\mu_i + \phi_i)(T - t_k)} - e^{-(\mu_i + \phi_i) \max\{\tau_{ij} - t_k, 0\}} \right] \right. \\ &\quad \left. + \left[ (T - t_k) e^{-(\mu_i + \phi_i)(T - t_k)} - \max\{\tau_{ij} - t_k, 0\} e^{-(\mu_i + \phi_i) \max\{\tau_{ij} - t_k, 0\}} \right] \right\} \\ &\quad + \mu_i \sum_{j=1}^n \mathbb{1}_{[\tau_{ij}, \infty)}(T) \sum_{k=1}^{n_{ij}} \frac{1}{\zeta_{ij}(k)} \frac{\partial}{\partial \phi_i} \psi_{ij}(k). \end{aligned}$$

In the above expression, the partial derivative of  $\psi_{ij}(k)$  with respect to  $\mu_i$  and  $\phi_i$  is computed recursively as follows:

$$\begin{aligned} \frac{\partial}{\partial \mu_i} \psi_{ij}(k) &= \frac{\partial}{\partial \phi_i} \psi_{ij}(k) = e^{-(\mu_i + \phi_i)(t_{\ell_k} - t_{\ell_{k-1}})} \left\{ \frac{\partial}{\partial \phi_i} \psi_{ij}(k-1) - (t_{\ell_k} - t_{\ell_{k-1}}) [1 + \psi_{ij}(k-1)] \right\} \\ &\quad - \sum_{h=\ell_{k-1}+1}^{\ell_k-1} (t_{\ell_k} - t_h) e^{-(\mu_i + \phi_i)(t_{\ell_k} - t_h)}, \end{aligned}$$

Similar considerations can be made for the partial derivatives with respect to  $(\nu_i, \theta_i)$  and  $(\nu'_j, \theta'_j)$ . In this case, the recursive form stems from  $\tilde{\psi}_{ij}(k)$ , which is function of the two pairs of parameters. For  $\nu_i$  and  $\theta_i$ :

$$\begin{aligned} \frac{\partial}{\partial \nu_i} \log L(\mathcal{H}_T | \Psi) &= \sum_{j=1}^n \frac{\mathbb{1}_{[\tau_{ij}, \infty)}(T) \nu'_j}{\nu_i + \theta_i} \sum_{k=1}^{n_{ij}} \left\{ \frac{\theta_i}{(\nu_i + \theta_i)(\nu'_j + \theta'_j)} \left[ e^{-(\nu_i + \theta_i)(\nu'_j + \theta'_j)(T - t_{\ell_k})} - 1 \right] \right. \\ &\quad \left. - \nu_i (T - t_{\ell_k}) e^{-(\nu_i + \theta_i)(\nu'_j + \theta'_j)(T - t_{\ell_k})} \right\} + \sum_{j=1}^n \sum_{k=1}^{n_{ij}} \frac{\mathbb{1}_{[\tau_{ij}, \infty)}(T) \nu'_j}{\zeta_{ij}(k)} \left[ \tilde{\psi}_{ij}(k) + \nu_i \frac{\partial}{\partial \nu_i} \tilde{\psi}_{ij}(k) \right], \\ \frac{\partial}{\partial \theta_i} \log L(\mathcal{H}_T | \Psi) &= - \frac{\nu_i}{\nu_i + \theta_i} \sum_{j=1}^n \mathbb{1}_{[\tau_{ij}, \infty)}(T) \nu'_j \sum_{k=1}^{n_{ij}} \left\{ \frac{1}{(\nu_i + \theta_i)(\nu'_j + \theta'_j)} \left[ e^{-(\nu_i + \theta_i)(\nu'_j + \theta'_j)(T - t_{\ell_k})} - 1 \right] \right. \\ &\quad \left. + (T - t_{\ell_k}) e^{-(\nu_i + \theta_i)(\nu'_j + \theta'_j)(T - t_{\ell_k})} \right\} + \nu_i \sum_{j=1}^n \sum_{k=1}^{n_{ij}} \frac{1}{\zeta_{ij}(k)} \frac{\partial}{\partial \theta_i} \tilde{\psi}_{ij}(k). \end{aligned}$$

The recursive equations for the partial derivative of  $\tilde{\psi}_{ij}(k)$  with respect to  $\nu_i$  and  $\theta_i$  are equivalent. For  $\theta_i$ :

$$\frac{\partial}{\partial \theta_i} \tilde{\psi}_{ij}(k) = e^{-(\nu_i + \theta_i)(\nu'_j + \theta'_j)(t_{\ell_k} - t_{\ell_{k-1}})} \left\{ \frac{\partial}{\partial \theta_i} \tilde{\psi}_{ij}(k-1) - (\nu'_j + \theta'_j)(t_{\ell_k} - t_{\ell_{k-1}}) [1 + \tilde{\psi}_{ij}(k-1)] \right\},$$

Similarly to the previous cases, the initial conditions is:

$$\frac{\partial}{\partial \theta_i} \tilde{\psi}_{ij}(1) = 0.$$